



Application of a Simplified Anisotropic Constitutive Model for Soft Structured Clay on Embankment Failure

Ali Shirmohammadi¹; Masoud Hajialilue-Bonab²; and Davood Dadras-Ajirloo³

Abstract: The design and maintenance of embankments is still a challenge in practical geotechnical engineering because of some features of soft sensitive soil behavior that are not considered in conventional methods. These features originate from the soil structure, including soil anisotropy, interparticle bonding, and decay as a result of the loading and deformation process. In recent years, many efforts have been made to incorporate the aforementioned features in various soil constitutive models. However, their application in practical geotechnical engineering is limited, owing to the complexity of the models, a number of parameters, and difficulties in the implementation in a computer code. The aim of this study is to modify a simple anisotropic constitutive model (SANICLAY) in order to take into account destructuration, named SANICLAY-D, and its implementation in computer code with a simple and robust algorithm. The capability of the proposed soil model in simulating the effects of the aforementioned soil features on the behavior of the well-known Test Embankment A constructed at Saint-Alban, Quebec, Canada, is explored. This model predicts, with sufficient accuracy, the effect of anisotropy on embankment failure behavior, especially the height and the failure surface, despite its simplicity. **DOI:** 10.1061/(ASCE)GM.1943-5622.0002109. © 2021 American Society of Civil Engineers.

Author keywords: Soft structured clay; Constitutive model; Anisotropy; Destructuration; Numerical simulation; Embankment; Failure.

Introduction

The numerical modeling and calculation of the response of geostructures constructed on soft, sensitive soil still remains a challenge in practical geotechnical engineering. This is due to the strong dependence of the mechanical behavior of these types of soil on the soil structure, which is not considered in conventional deformation and limit equilibrium analyses. Neglecting the effects of the soil structure may lead to inaccurate prediction of the behavior of geostructures built on soft soils.

The soil structure is usually referred to as a combination of fabric (spatial particle arrangement) and interparticle bonding (Lambe and Whitman 1991; Mitschell and Soga 2005). The fabric is an outcome of the deposition process and is affected by the rate of sedimentation and the consolidation history. Owing to K_0 consolidation, the fabric exhibits a particular orientation that renders the behavior of soil different in the consolidation direction, compared with the other directions. The interparticle bonding develops as a result of the chemical process and causes intact natural soils to be bulky and exist at a higher void ratio than a remolded and disturbed soil under the same effective stress. This component of the

Note. This manuscript was submitted on May 6, 2020; approved on March 19, 2021; published online on May 19, 2021. Discussion period open until October 19, 2021; separate discussions must be submitted for individual papers. This paper is part of the *International Journal of Geomechanics*, © ASCE, ISSN 1532-3641.

soil structure is more sensitive to loading and can easily degrade during the deformation process. The progressive breakage of interparticle bonding is called destructuration. Anisotropy and destructuration have remarkable effects on the strength and mechanical behavior of soft soils and must be considered in practical geotechnical engineering.

To this end, in the past decade, much effort has been put into the development and extension of constitutive models to incorporate the features of soil structure in the simulation of the behavior of soft soils. Yet few models cover the combined effect of anisotropy and destructuration. One relatively simple way to consider the anisotropy of the fabric and its evolution as the result of loading and plastic straining is the employment of an inclined yield surface and a rotational hardening rule. This framework of the constitutive modeling of cross anisotropy was first laid out by Dafalias (1986a) and has since been applied by other researchers in the development of anisotropic soil models (Korhonen and Lojander 1987; Newson and Davies 1996; Thevanayagam and Chameau 1992; Wheeler et al. 2003). A popular framework in capturing the effects of the interparticle bonding and its breakage on natural soils was first introduced by Gens and Nova (1993) and comprises two main points: the role of the yield surface in identifying the onset of destructuration and evaluation of natural soil behavior with respect to the equivalent remolded soil. Based on this framework, several constitutive models have been extended to incorporate interparticle bonding and the effect of its decay (Baudet and Stallebrass 2004; Karstunen et al. 2005; Rouainia and Muir Wood 2000). In all of these models, the destructuration rule has an isotropic softening mechanism and is defined as isotropic reduction of the size of the expanded yield surface. Taiebat et al. (2010) proposed a novel destructuration rule, called frictional destructuration, in which an enlarged critical stress ratio due to the existence of the soil structure reduces with plastic straining. Taiebat et al. (2010) added an isotropic and frictional destructuration rule to the Simple Anisotropic Clay (SANICLAY) model and successfully simulated the behavior of Bothkennar clay reported by Smith et al. (1992). This model is referred to as the SANICLAY-D model.

¹Ph.D. Student, Dept. of Geotechnical Engineering, Faculty of Civil Engineering, Univ. of Tabriz, Tabriz 5165656361, Iran. ORCID: https://orcid.org/0000-0002-4455-4983. Email: a.shirmohammadi@tabrizu.ac.ir

²Professor, Dept. of Geotechnical Engineering, Faculty of Civil Engineering, Univ. of Tabriz, Tabriz 5165656361, Iran (corresponding author). ORCID: https://orcid.org/0000-0003-2865-2492. Email: hajialilue@tabrizu.ac.ir; mhbonab@gmail.com

³Ph.D. Student, Dept. of Civil and Environmental Engineering, Norwegian Univ. of Science and Technology (NTNU), Trondheim 7491, Norway. ORCID: https://orcid.org/0000-0002-8245-8124. Email: davood.dadrasajirlou@ntnu.no

In 1972, the geotechnical group of Laval University conducted a comprehensive research program on the behavior of embankments on soft, sensitive soils. In this project, four fully instrumented trial embankments were built on the soft Champlain deposit in Saint-Alban, Quebec, Canada. This study produced a very valuable set of data on different aspects of the behavior of embankments and their soft soil foundations for the validation of different modeling methods. Embankment A, one of these four embankments, which was built until failure occurred in the soft soil foundation, is selected in this paper for coupled finite-difference analysis with a simple anisotropic constitutive model for soft, sensitive soils. Several researchers have previously analyzed this embankment. Hight (1998) and Zdravković et al. (2002) were among the first researchers to apply an advanced constitutive model to simulate the embankment behavior. They employed the MIT-E3 model (Whittle and Kayvadas 1994) besides the classical Modified Cam-Clay model (MCC) in plane-strain finite-element analyses and concluded that the effect of anisotropy on the mobilized strength along the failure surface has an important role in the correct prediction of the failure height and the behavior of the embankment. Despite the satisfactory results of the simulation, the destructuration of soft, sensitive Champlain soil was not considered in their analyses. Moreover, in their analyses it was assumed that embankment fills were constructed in undrained conditions. Yet the occurrence of consolidation, particularly in the early stages of construction, has a considerable effect on the stress path followed by the soil elements beneath the embankment (Leroueil et al. 2001). Grammatikopoulou et al. (2007) performed a series of plane-strain finite-element analyses of the embankment under undrained conditions and investigated the effect of the shapes of yield and plastic potential surfaces in the deviatoric plane on the behavior of the embankment. They also neglected the effect of soil structure and used the bubble model (Al-Tabbaa and Wood 1989) with isotropic strength in their analyses. Their conclusions supported the work of Potts and Gens (1984), finding that different shapes for the plastic potential and yield surfaces in the deviatoric plane should be adopted in plane-strain analyses. Andresen et al. (2011) also modeled the Saint-Alban embankment with a plane-strain finite-element method under undrained conditions using the Norwegian Geotechnical Institute-active, direct simple shear, passive (NGI-ADP) model, an anisotropic soil model that directly accepts undrained shear strength as an input parameter. The destructuration of the soft soil and u-p (pore pressure–displacement) coupled analysis were not taken into account in their studies. The prediction of slip surface was significantly different from field observations and the simulated horizontal displacement was greater than in field measurements. Panayides et al. (2012) studied the influence of destructuration on the behavior of the embankment with coupled plane-strain finite-element analyses using the Kinematic Hardening Constitutive Model (KHCM) for natural clays (Rouainia and Muir Wood 2000), with very similar functionality to the bubble model. In the KHCM, anisotropy is assumed to originate from interparticle bonding and the decay of this constituent of the soil structure erases the anisotropy. The results of the simulations of Panayides et al. (2012) are more consistent with the field data than those of previous studies. Still, there are remarkable discrepancies between the predicted slip surface and the actual slip surface observed at the site (Rochelle et al. 1974).

Most of the aforementioned complex constitutive models used for the simulation of foundation soil of Embankment A do not consider anisotropy and destructuration features of the soil structure together. Also, their numerical implementation in numerical codes is relatively complicated. In this study, the performance and capability of the SANICLAY-D model in reproducing the behavior of Test Embankment A is explored through a series of coupled plane-strain

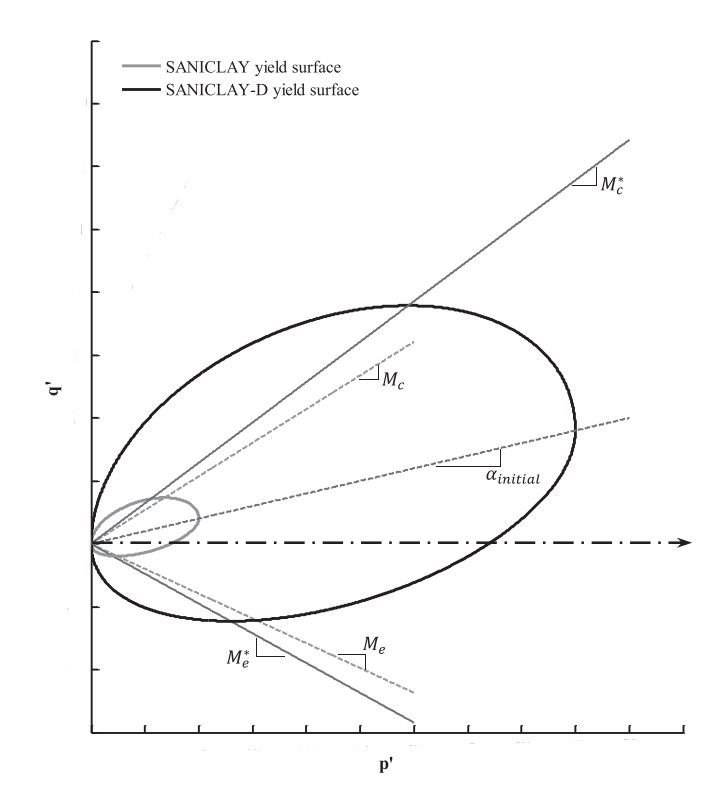


Fig. 1. SANICLAY and SANICLAY-D initial yield surfaces.

finite-difference analyses. To this end, a simple and robust algorithm for the implementation of the SANICLAY-D model into Fast Lagrangian Analysis of Continua (FLAC) code is presented (version 8.0, Itasca, Minneapolis, Minnesota), which makes the model very attractive from a practical point of view. In addition, the effects of anisotropy and destructuration of the soft foundation soil on the behavior of the embankment are investigated.

Simplified Anisotropic Model for Clay Formulation

The SANICLAY-D model is an extension of the original SANI-CLAY model (Dafalias et al. 2006; Taiebat et al. 2010), with a modified rotational hardening rule proposed by Dafalias and Taiebat (2013). This modification was recently approved in convergence by Dafalias et al. (2020). Taiebat et al. (2010) extended the original SANICLAY model by including destructuration theory. In this study, the model proposed by Dafalias and Taiebat (2013) is extended according to the decay of a clay structure proposed by Taiebat et al. (2010). In the SANICLAY-D model, the yield surface for naturally structured clay is defined as the expansion of the yield surface for the corresponding reconstituted soil using frictional (S_f) and isotropic (S_i) structuration factors (Fig. 1). The sheared ellipsoid yield surface of the model in three-dimensional (3D) stress space can be expressed as

$$f = \frac{3}{2}(\mathbf{s} - p\boldsymbol{\alpha}) : (\mathbf{s} - p\boldsymbol{\alpha}) - \left(S_f^2 M(\theta)^2 - \frac{3}{2}\boldsymbol{\alpha} : \boldsymbol{\alpha}\right) p(S_i p_0 - p) = 0$$
(1)

where p and s = mean pressure and the deviatoric stress, respectively, given by

$$p = \frac{1}{3}tr[\boldsymbol{\sigma}], \qquad s = \boldsymbol{\sigma} - p\boldsymbol{I}$$
 (2)

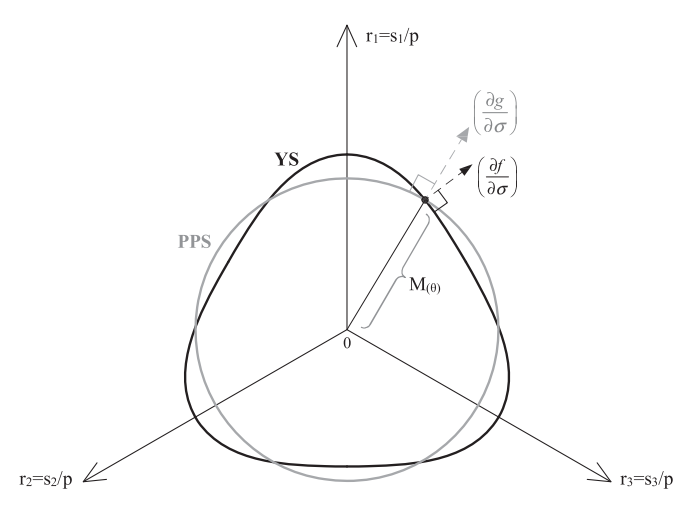


Fig. 2. Yield and PPSs of SANICLAY-D model in deviatoric plane.

where $\mathbf{I} = \text{second-rank}$ identity tensor and $tr[\]$ is the trace operator; $\boldsymbol{\alpha} = \text{deviatoric}$ dimensionless fabric tensor; $p_0 = p\text{-coordinate}$ of the intersection of the line with slope α and the intrinsic yield surface that controls the size of the surface; and $M(\theta) = \text{slope}$ of the critical state line and determines the shape of the surface in the deviatoric plane. Using the proposition of Sheng et al. (1999), $M(\theta)$ can be expressed as the function of the Lode angle:

$$M(\theta) = M_c \left(\frac{2m^4}{1 + m^4 - (1 - m^4)\sin 3\theta}\right)^{1/4} \tag{3}$$

where $m = M_e/M_c$, M_e and M_c = critical stress ratios for triaxial extension and compression respectively; θ =Lode angle and can be defined as

$$\theta = \frac{1}{3}\sin^{-1}\left(\sqrt{6}tr[\mathbf{n}^3]\right), \qquad \mathbf{n} = \frac{\mathbf{r} - \boldsymbol{\alpha}}{[(\mathbf{r} - \boldsymbol{\alpha}):(\mathbf{r} - \boldsymbol{\alpha})]^{1/2}}$$
(4)

where r = s/p = deviatoric stress ratio tensor. A simple nonassociated flow rule has been adopted in this study, in which the shape of the plastic potential surface (PPS) in the deviatoric plane is circular and in the meridian is a distorted or rotated ellipse with similar rotation of the yield surface. For a general stress state on the yield surface (YS), the value of M in the PPS is also determined using Eq. (3). The plastic potential will pass through the current stress state (Fig. 2) regarded as independent of the Lode angle when the derivatives of the PPS are evaluated with respect to the stresses. Hence, the value of p_0 is equal for both yield and potential surfaces. Assuming a circular shape for the plastic potential in the deviatoric plane not only simplifies the implementation of the model but also has a dominating influence on the predicted behavior for plane-strain problems (Potts and Gens 1984). In this regard, Grammatikopoulou et al. (2007) conducted a number of plane-strain finite-element analyses of Embankment A, the analysis of which is the subject of this work, and investigated the effect of yield and plastic potential deviatoric surfaces on the behavior of the embankment. Grammatikopoulou et al. (2007) employed an isotropic strength constitutive model and explored different scenarios for the yield and PPS shapes in the deviatoric plane. It was discovered that the correct failure height for the embankment is predicted when the yield and PPSs have Mohr-Coulomb hexagonal and circular shapes, respectively, in the deviatoric plane.

To describe the development or erasure of fabric anisotropy with plastic strain, Dafalias and Taiebat (2013) proposed a new rotational hardening rule that yields a unique critical state line in e-ln(p) space in regard to loading at different Lode angles, which

can be expressed as

$$\dot{\alpha} = \langle L \rangle C p_{atm} \left(\frac{p}{S_i p_0} \right) (\alpha_b^* - \alpha) + \left(\frac{\dot{S}_f}{S_f} \right) \alpha \tag{5a}$$

$$\alpha_b = \sqrt{\frac{2}{3}} \left(\frac{M(\theta)}{z} \right) \left[1 - \exp\left(-s \left(\frac{|\eta|}{M(\theta)} \right) \right) \right] n_r \tag{5b}$$

$$\alpha_b^* = S_f \alpha_b = S_f \sqrt{\frac{2}{3}} \left(\frac{M(\theta)}{z} \right) \left[1 - \exp\left(-s \left(\frac{|\eta|}{M(\theta)} \right) \right) \right] n_r \qquad (5c)$$

where L= plastic multiplier and is enclosed in the Macauley brackets $\langle \rangle$ to discriminate plastic loading (L>0) from elastic unloading (L<0); and C= model parameter controlling the rate of the evolution of α to its bounding value α_b^* . In Eq. (5b), s and z= model parameters, regulating the equilibrium values of α under constant stress ratio loading, $\eta=\sqrt{(3/2)\text{tr}[r^2]}$; and $n_r=r/|r|=$ unit norm deviatoric tensor along deviatoric stress ratio r. It should be noted that in Eq. (5c) S_f is multiplied by α_b for the limitation of excessive rotation and the approach of α_b^* to $S_fM(\theta)$. According to Taiebat et al. (2010), the second term in Eq. (5a) prevents α from having a value greater than $S_fM(\theta)$, owing to frictional destructuration, which is a prerequisite for the definition of the yield and potential surfaces.

A summary of the destructuration hardening rules and the volumetric hardening equation is presented in the Appendix for the sake of completeness.

Implementation of the SANICLAY-D Model

The SANICLAY-D model has been numerically implemented as a user-defined model (UDM) into the two-dimensional (2D) finitedifference code FLAC. The constitutive model is written in C++ programming language and compiled as a dynamic link library (DLL) file. FLAC, which has been proved to be an effective and powerful tool for solving complex geostructure problems using UDMs (Razavi et al. 2020; Rotisciani and Miliziano 2014), employs the explicit central finite-difference method to solve the dynamic equation of motion, even for static problems, at every grid point resulting from discretization of the soil region with quadrilateral elements. In fact, FLAC utilizes a time-marching method for modeling wave transmission through the body whose load-deformation response is the subject of engineering analyses. In such methods, during one solution step, none of the elements interacts with any of the other elements and, consequently, a very small time step is prerequisite to the computational stability of the global solution. In this regard, the time step must be less than a critical value in order to ensure that the computational wave speed always stays ahead of the physical wave speed (version 8.0, Itasca, Minneapolis, Minnesota). The critical time step is a function of the properties of numerical models, such as element size, material and structure stiffness, permeability, and damping. Under such a condition, the use of implicit methods for stress integration is quite unnecessary. Therefore, an explicit form of the integration scheme of constitutive models can be employed. In this work, an explicit forward Euler method with single-step plastic correction without any iterative process was utilized.

In this regard, according to Rousé et al. (2006) and Rotisciani and Miliziano (2014), there are two simple and efficient approaches for implementing constitutive models with a specified YS within FLAC using a single-step plastic correction method. Both methods involve determining the plastic multiplier for the calculation of the plastic corrector. In the first approach, which is applicable to constitutive models with a general form of YS, the plastic multiplier is calculated by enforcing the consistency condition, df = 0. The

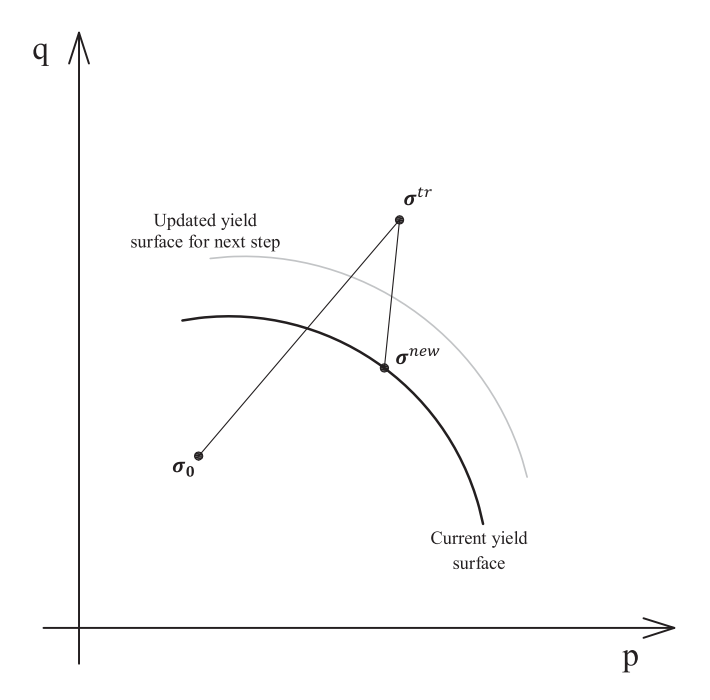


Fig. 3. Single-step plastic correction semiexplicit method.

consistency condition is the term used to indicate the requirement for the stress state to remain on the YS during plastic deformation. In the other approach, which has been employed within FLAC for the implementation of the MCC model, the plastic multiplier is computed by setting the YS function equal to zero at the stress state obtained from the plastic correction, $f(\sigma_0 + d\sigma) = 0$. This approach should be used with the constitutive models with simple YS; that is, the equation $f(\sigma_0 + d\sigma) = 0$ leads to a simple equation in terms of the plastic multiplier whose solution does not require iterative numerical methods (Fig. 3). Shirmohammadi et al. (2016) called this approach a semiexplicit method and applied it for the implementation of the original SANICLAY model. The pseudocode in Fig. 4 describes the implementation into FLAC of the SANICLAY-D model in general stress space using the semiexplicit method. As can be seen in Fig. 4, the implementation process is categorized into two sets of operations. This is because of the application of mixed discretization techniques (Morti and Cundall 1982) in FLAC code to restrain zero-energy mode deformations and overcome mesh-locking problems by subdividing each quadrilateral element into two overlaid sets of constant strain triangular subelements. In the mixed discretization technique, the number of degrees of freedom increases through the utilization of different discretizations for volumetric (isotropic) and deviatoric components of strain and stress in which the isotropic parts of the strain and stress tensors are computed with a weighted average scheme and kept constant for the whole quadrilateral element, while the deviatoric parts are treated independently for each subelement. As a consequence, constitutive models in FLAC code operate four times in each quadrilateral element for every time step. Similar to the isotropic parts of the strain and stress tensors, the increments of hardening parameters of constitutive models must be averaged over four subelements, since deviatoric hardening parameters are updated and stored in subzones, while the volumetric hardening parameter has been updated and stored only once per quadrilateral element.

Ground Condition at Saint-Alban

The Champlain clay deposit is a soft, sensitive soil with postsedimentation structure (Cotecchia and Chandler 2000) that has a

fragile porous matrix, developed as a result of a combination of factors, such as the salinity of the environment, the presence of some bonding agent, such as glacially ground amorphous materials (alumina, iron, and silica), and rapid sedimentation (Quigley 1980). Consequently, high compressibility and sensitivity, low shear strength, and cross anisotropy are among the most common features of the behavior of the Champlain clay deposit.

The fairly uniform soil profile at Saint-Alban comprises an approximately 2.0 m thick weathered clay crust and an 8.0 m thick soft silty marine clay deposit, below which there is a layer of clayey silt with sand, extending to 13.7 m depth. This is underlain by a fine to medium sand, which extends to a depth of 24.4 m. The groundwater table is close to 0.7 m below ground level and the in situ pore pressures increases from that level. The underlying soft silty marine clay is lightly overconsolidated, with an overconsolidation ratio (OCR) of around 2.2. The bulk unit weights of the soil above the water level were measured as 19 kN/m³ and below it as 16 kN/m³ (Rochelle et al. 1974).

To evaluate the aforementioned features, extensive laboratory and field experiments were conducted at the Saint-Alban site. Laboratory experiments mainly consisted of isotropically consolidated undrained (CIU) and unconsolidated undrained (UU) triaxial tests (Tavenas and Leroueil 1977), along with direct simple shear (DSS) tests (Lefebvre and Pfendler 1996), while the vane shear test (VST) was mostly used as an in situ experiment (Rochelle et al. 1974).

The undrained shear strength (S_u) profiles determined from the aforementioned laboratory and field tests (Trak et al. 1980), as well as those obtained from numerical simulations, are shown in Fig. 5. As can be seen, laboratory tests overall gave higher values for S_u than field tests (VST). This was diagnosed by Rochelle et al. (1974) as the effect of soil anisotropy and soil disturbance, owing to intrusion of the vane into the soil, which, to some extent, may cause damage to the soil structure.

A coefficient of earth pressure at rest $(K_0^{\rm NC})$ for normally consolidated Champlain clay was estimated as 0.546 using the empirical relation, $K_0^{\rm NC}=1-\sin\phi_{\rm TC}'$, corresponding to an effective friction angle in triaxial compression, $\phi_{\rm TC}'=27^{\circ}$. The permeability of the Champlain clay was reported to be around 10^{-10} to 10^{-9} m/s by Tavenas et al. (1983). A uniform medium to coarse sand, containing about 10% fine sand and 10% gravel, is the fill material of the embankment, and the bulk unit weight was measured as 19 kN/m³. Triaxial tests were conducted at the confining pressure equal to the mean effective stress in the fill on the samples that were prepared at similar densities to that of the field, giving a friction angle $\phi_{\rm TC}'$ of 44° and a dilation angle of 22°.

Geometry and Construction Stage of Test Embankment A

To persuade failure to occur in a specified direction, a berm was created at a height of 1.5 m on the right side of the embankment. For the same reason, three sides of the embankment had a 2:1 slope, yet the fourth face of the embankment had a steeper slope of 1.5:1 inclination. Under such conditions, limit equilibrium analysis proved that Test Embankment A could be constructed to a height of 4.6 m, with a crest length of 30.5 m and a width of 7.6 m. The described geometry for the embankment is given in Fig. 6(a).

According to Rochelle et al. (1974), on the first day, 0.6 m of sand fill was placed and compacted, and then a layer of 0.3 m per day was added until a height of 1.5 m was reached. After that, two 0.3 m layers were placed per day until failure occurred

Operations within each of 4 triangular sub-elements inside a quadrilateral element:

- 1. Initialize the model parameters; this step is only executed once when the model is assigned.
- 2. Obtain strain increment $(d\varepsilon)$ and decompose it into the volumetric $(d\varepsilon_p)$ and deviatoric $(d\varepsilon_s)$ components.
- 3. Calculate elastic predictor or trial stress state:

$$\sigma^{tr} = s^{tr} + p^{tr}I$$

$$s^{tr} = s^{0} + 2Gd\varepsilon_{s}$$

$$p^{tr} = p^{0} + Kd\varepsilon_{p}$$

where p^0 and s^0 are the volumetric and deviatoric components of initial stress state, respectively.

- 4. Check yield criterion at trial stress state and initial hardening parameters $f(\sigma^{tr}, q^0)$, q^0 is initial hardening parameter that can be tensor or scalar quantity:
 - a. If $f(\sigma^{tr}, q^0) > 0$ then
 - i. Calculate plastic multiplier (L) by solving the quadratic equation below in terms of L for the smallest positive root:

$$(A)L^{2} + (B)L + C = 0$$

$$A = \frac{3}{2} \left[K \left(\frac{\partial g}{\partial p} \right)^{tr} \alpha - 2G \left(\frac{\partial g}{\partial s} \right)^{tr} \right] : \left[K \left(\frac{\partial g}{\partial p} \right)^{tr} \alpha - 2G \left(\frac{\partial g}{\partial s} \right)^{tr} \right]$$

$$+ \left[S_{f}^{2} (M^{tr}(\theta))^{2} - \frac{3}{2} (\alpha; \alpha) \right] \left[K \left(\frac{\partial g}{\partial p} \right)^{tr} \right]^{2}$$

$$B = 3(s^{tr} - p^{tr}\alpha) : \left[K \left(\frac{\partial g}{\partial p} \right)^{tr} \alpha - 2G \left(\frac{\partial g}{\partial s} \right)^{tr} \right] - K \left(\frac{\partial g}{\partial p} \right)^{tr} (S_{i}p_{0} - 2p^{tr}) \left[S_{f}^{2} (M^{tr}(\theta))^{2} - \frac{3}{2} (\alpha; \alpha) \right]$$

$$C = f(\sigma^{tr}, q^{0})$$

The above quadratic equation has been obtained by enforcing $f(\sigma^n, q^0) = 0$ and some manipulation afterwards, where:

$$\sigma^n = s^n + p^n I \tag{a}$$

$$s^{n} = s^{tr} - 2GL \left(\frac{\partial g}{\partial s}\right)^{tr} \tag{b}$$

$$p^{n} = p^{tr} - KL \left(\frac{\partial g}{\partial p}\right)^{tr} \tag{c}$$

$$\begin{split} &\left(\frac{\partial g}{\partial p}\right)^{tr} = S_f^2 (M^{tr}(\theta))^2 - \frac{3}{2} (\boldsymbol{r}^{tr} : \boldsymbol{r}^{tr}) \\ &\left(\frac{\partial g}{\partial s}\right)^{tr} = 3p^{tr} (s^{tr} - p^{tr} \boldsymbol{\alpha}) \\ &\boldsymbol{r}^{tr} = \frac{s^{tr}}{n^{tr}} \end{split}$$

- ii. Apply the plastic corrector and calculate new stress state using equations a, b and c.
- iii. Calculate increment of hardening parameters, dq.
- iv. Update the rotational hardening parameters: $q = q + \overline{dq}$
- b. Else

No plastic response takes place, thus:

$$\sigma^{n} = s^{n} + p^{n}I$$

$$s^{n} = s^{tr}$$

$$p^{n} = p^{tr}$$

5. Deliver new stress state to FLAC.

Operations referring to the whole quadrilateral element composed of 4 triangular sub-elements:

- 6. After the above operations for each triangular sub-element have completed, the area-weighted average value of the following variables corresponding to the quadrilateral element are calculated:
 - Volumetric strain increment $(\overline{d\varepsilon}_p)$
 - Increments of hardening parameters (\overline{dq}) , if plastic response took place in any of triangular sub-elements
 - Mean effective stress (\bar{p})
- 7. Update the following variables
 - Hardening parameters and state variables: $q = q + \overline{dq}$

Calculate elastic bulk and shear moduli needed for the computation of time step size.

Fig. 4. Pseudocode for the implementation of the SANICLAY-D model into FLAC.

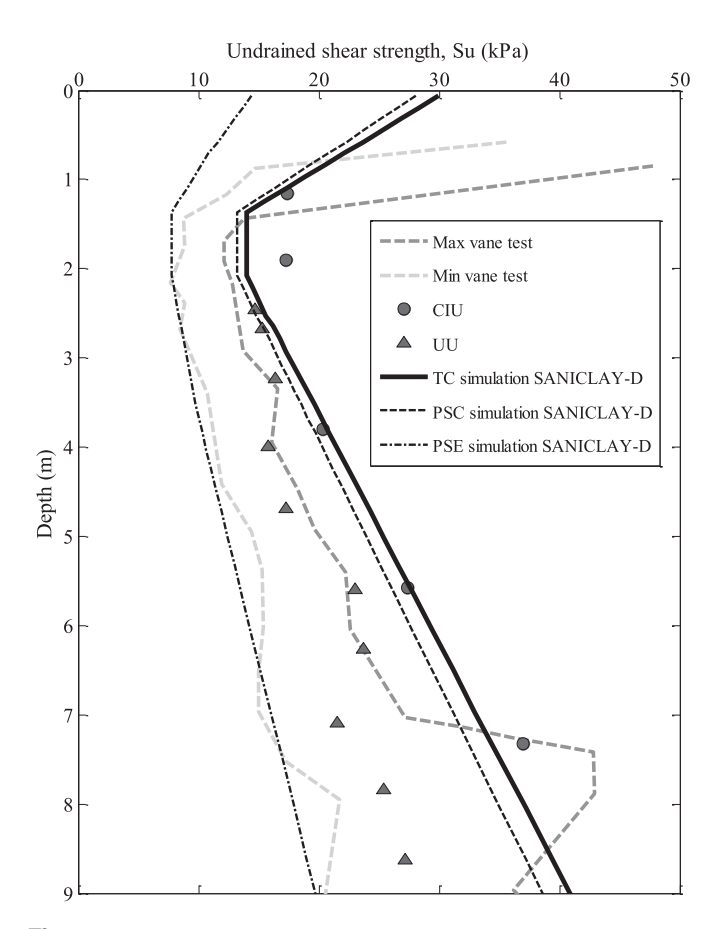


Fig. 5. Experimented and simulated undrained strength profiles for soft Champlain clay at Saint-Alban. (Data from Trak et al. 1980.) PSC = plane stress compression; PSE = plane stress extension; TC = triaxial compression.

at an embankment height of about 3.9 m. Each layer of fill was compacted with the same energy as the initial 0.6 m to ensure uniform density.

To record details of the deformations and excess pore water pressure, a number of instruments were installed within and beyond the unsupported side of the embankment. Ten fragile wooden sticks of 5.5 m long (L1–L10) were installed in the ground at and beyond the toe of the test embankment to determine the location and shape of the failure surface [Fig. 6(b)]. The two sets of displacement gauges designated R1–R15 and R16–R27 were installed within the embankment and beyond its toe, respectively. The second set was placed in position after 0.6 m fill of sand.

Soil Properties and Model Parameter Calibration

The SANICLAY-D model requires ten material and three initial state parameters. They are listed with their descriptions and values for soft Champlain clay in Table 1. The parameters κ^* , λ^* , ν , and M_c (M_e) are related to the critical state soil mechanics. The additional parameters s and z are rotational hardening parameters, which limit excessive rotation of the YS under constant stress ratio loading. The remaining three model parameters, namely k_i , k_i , and k_i , describe the decay of the soil structure.

The aforementioned parameters can be straightforwardly determined. The slope of the critical state line (CSL) in compression (M_c) and extension (M_e) can be obtained indirectly from the

reported value of 27° for the internal frictional angle (ϕ'_c) as

$$M_c = \frac{6\sin\phi'}{3 - \sin\phi'}, \qquad M_c = \frac{6\sin\phi'}{3 + \sin\phi'}$$
 (6)

where λ^* and κ^* = gradients of the normal compression and swelling lines in a $\ln(\nu)$ - $\ln(p)$ plane, and their value has been measured from odometer test data conducted on samples retrieved from depths of 3.7 and 5.6 m, as reported by Tavenas et al. (1974). Poisson's ratio is assumed to be equal to 0.3, according to Tavenas et al. (1974).

For the estimation of the constants s and z, the K_0 -based procedure proposed by Dafalias and Taiebat (2013) has been followed. Under K_0 stress path loading, α asymptotically approaches K_0 anisotropy (α_{K_0}), which can be calculated as

$$\alpha_{K_0} = \frac{\eta_{K_0}^2 + 3\left[1 - \left(\frac{\kappa^*}{\lambda^*}\right)\right] \eta_{K_0} - M^2}{3\left[1 - \left(\frac{\kappa^*}{\lambda^*}\right)\right]}$$
(7)

where $\eta_{K_0} = K_0$ stress ratio given by

$$\eta_{K_0} = \frac{3(1 - K_0)}{(1 + 2K_0)} \tag{8}$$

Zeroing the rotational hardening equation leads to $\alpha_b = \eta_{K_0}$ and, by taking s = z as default choice, according to Dafalias and Taiebat (2013), s and z can be calibrated as

$$\alpha_b = \alpha_{K_0} = \frac{M}{z} \left[1 - \exp\left(-s \frac{|\eta_{K_0}|}{M}\right) \right]$$
 (9)

To evaluate the structural state parameters (S_i and S_f) and calibrate the destructuration parameters (k_i , k_f , and A), as well as the parameter C, which controls the pace of rotational hardening, CIU and DSS tests were conducted on samples retrieved from depths of approximately 3 and 5.7 m and have been simulated. Figs. 7 and 8, respectively, show the experimental and numerical simulations of three triaxial tests performed on the samples consolidated to pressures of 44, 66.6, and 77 kPa and of the DSS test. As can be seen, there is a reasonable agreement between the experimental data and the numerical simulations. From simulation of the aforementioned tests, the structural state parameters are estimated as $S_i = 4.5$ and $S_f = 1.165$. Finally, the values of calibrated parameters are given in Table 1.

Finite-difference Model

The finite-difference software FLAC 2D (version 8.0, Itasca, Minneapolis, Minnesota) was used to simulate the construction and failure of Test Embankment A. The finite-difference grid and its associated boundary conditions for plane-strain analysis are shown in Fig. 9. The lateral boundaries are fixed in the horizontal direction, whereas the bottom boundary is restricted against movement both vertically and horizontally. The distance of lateral boundaries from the nearest toe of the embankment is taken to be about 50.0 m, to limit the impact of the boundary condition on the result of the analyses. This was determined by trial and error, to achieve the state in which the rotation of principal stresses faded at the lateral boundaries. To produce accurate results, mesh sensitivity studies were carried out by constructing several models to ensure that the zone was sufficiently dense and fine.

The actual construction history of the embankment, which is illustrated in Fig. 10, was taken in the numerical model. In this regard, a simplified hydromechanical u-p coupling was employed, in

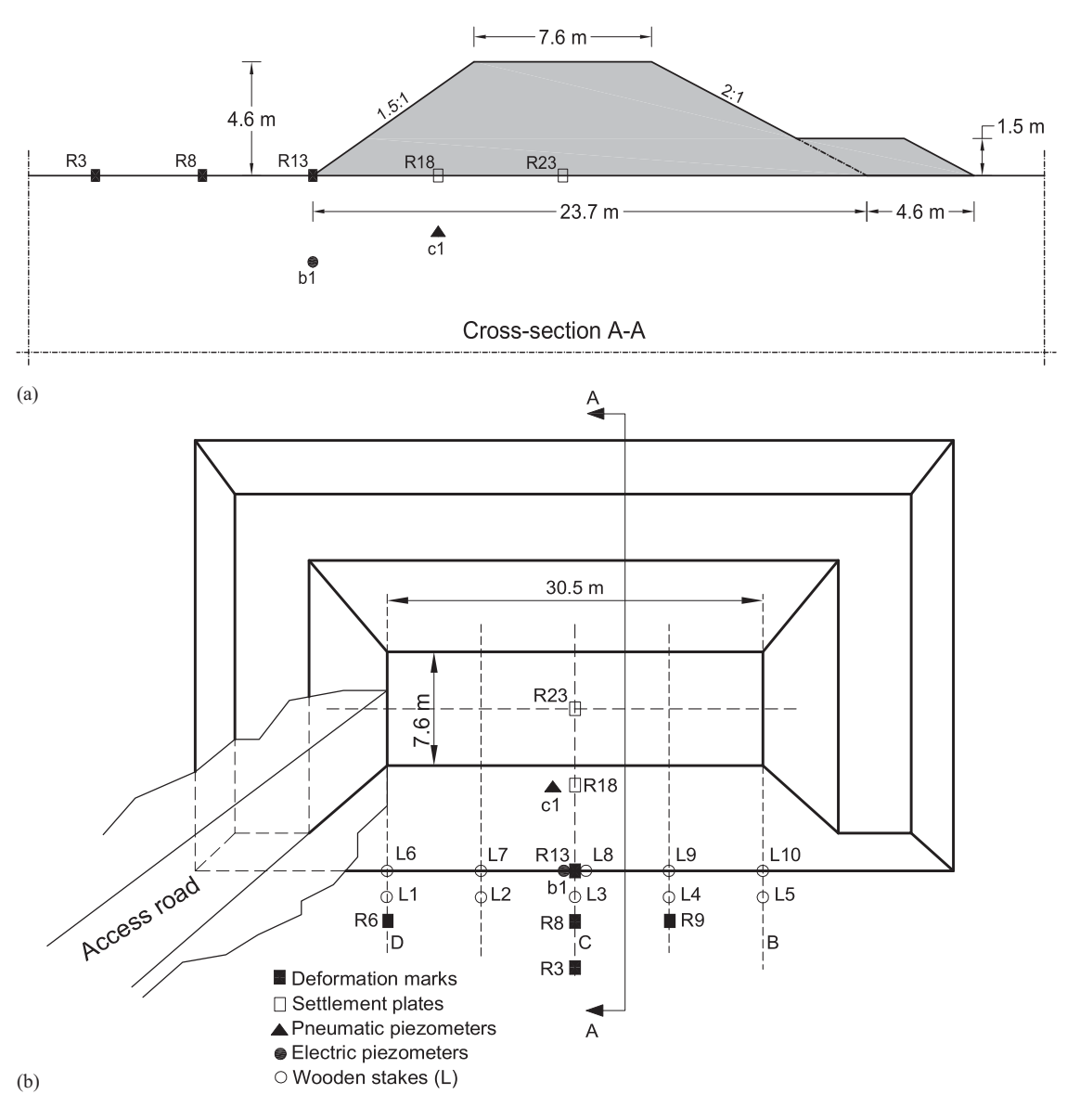


Fig. 6. Saint-Alban Test Embankment A: (a) cross section A-A; and (b) plan view.

which there were two simulation stages for the construction of each embankment layer. The first stage related to the instantaneous undrained response of the system. In this stage, it was assumed that no water flow occurred and excess pore water pressure was produced, owing to embankment lift placement. In the second stage, a transient fluid flow-only calculation was made and subsequently excess pore water pressure produced in the first stage dissipated through the soil above the water table. The water table level was assumed to be at a depth of 0.7 m beneath the ground surface.

Following previous studies (Zdravković et al. 2002; Grammatikopoulou et al. 2008; Panayides et al. 2012), the embankment fill material was modeled using a linear elastic and perfectly plastic nonassociated Mohr–Coulomb model using the parameters given in Table 2.

Results and Discussion

To show the effect of destructuration and anisotropy on the behavior of Embankment A and the capability of the SANICLAY-D model to simulate these features, three cases were considered for

numerical analysis. In the first case, the soil foundation behavior was simulated using the SANICLAY-D model, which incorporates both the destructuration and the anisotropy. In the second case, only the strength anisotropy was taken into account and then the SANICLAY model was used as a constitutive model for the soil foundation. Finally, in the last case, the MCC model was employed, which ignores both the strength anisotropy and the destructuration. The SANICLAY and MCC models are simplifications of the SANICLAY-D model. The SANICLAY model can be obtained by setting the initial values of the state parameters S_f and S_i as one. To further simplify the model to the MCC model, besides these settings, the initial value of the state parameter α and the model constant C were set to zero.

The results of the analyses of these cases are presented in terms of displacement, the shape of the slip surface, and excess pore water pressure.

Vertical and Horizontal Displacements

The vertical displacement at settlement gauges R23 and R18 against the embankment height were predicted by the three

Table 1. Parameters of the SANICLAY-D model with destructuration for Champlain clay

Constant type	Parameter	Description	Value	
Elasticity	K*	Elastic volume change due to a change in mean stress		
·	v	Poisson's ratio	0.3	
Critical state	M_c	Slope of the critical state line (compression)		
	λ^*	Slope of the normally consolidated line (NCL) in $ln(e)-ln(p')$ space		
	m(n)	Ratio of the slope of the critical state line (extension or compression)		
Rotational hardening	c	Rate of evolution of anisotropy		
	S	Rotational hardening parameter		
	z	Rotational hardening parameter		
Destructuration	k_i	Parameter describing the rate of isotropic destructuration		
	k_f	Parameter describing the rate of frictional destructuration		
	$\overset{{}_\circ}{A}$	Parameter describing coupling between volumetric and frictional destructuration		
State variables	α	Initial rotation of YS		
	S_i	Initial isotropic structuration factor		
	$\dot{S_f}$	Initial frictional structuration factor		

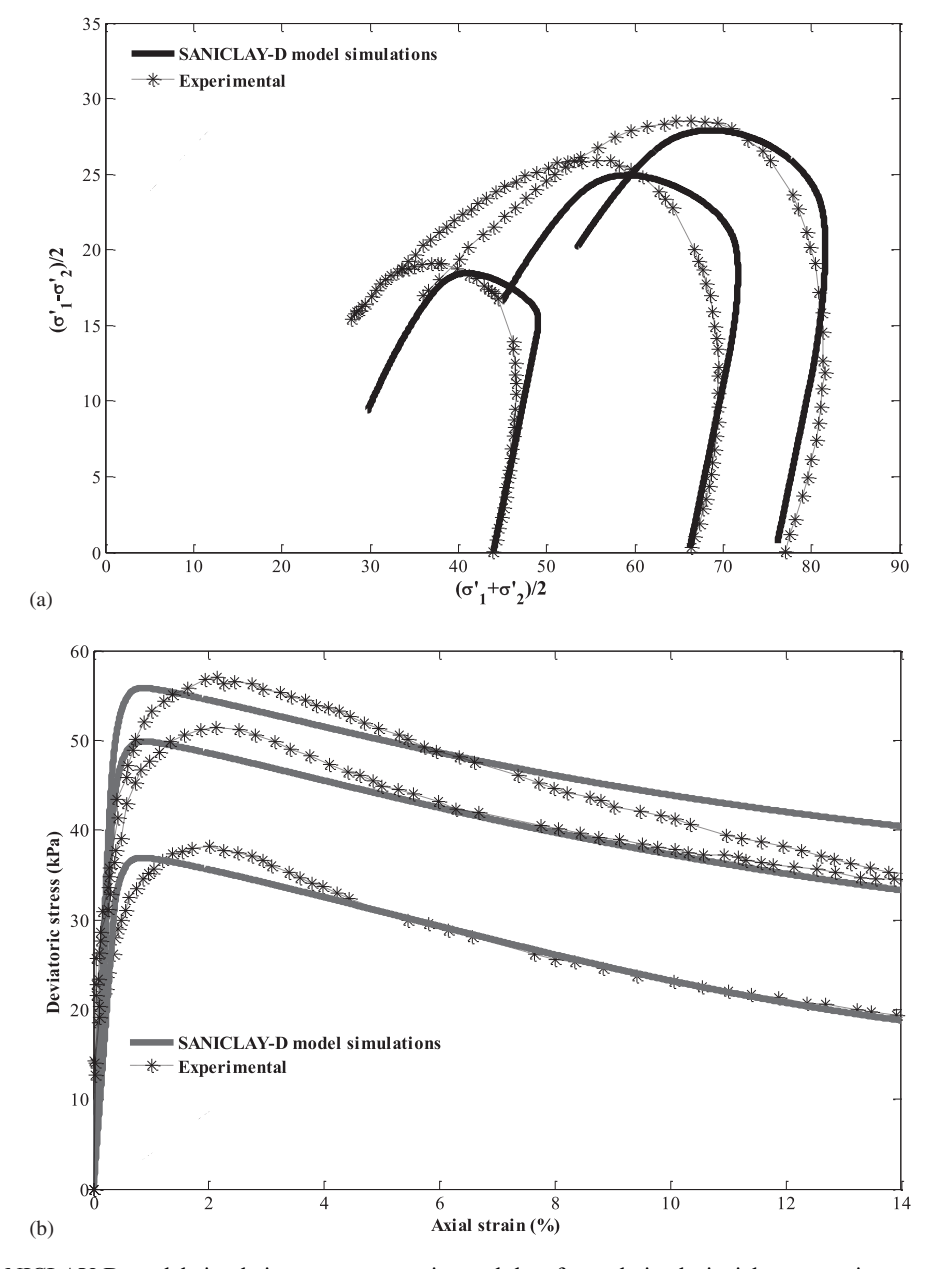


Fig. 7. Validation of SANICLAY-D model simulations versus experimental data for undrained triaxial compression tests on isotropically consolidated clay: (a) effective stress paths; and (b) deviator stress as a function of axial strain. (Data from Tavenas and Leroueil 1977.)

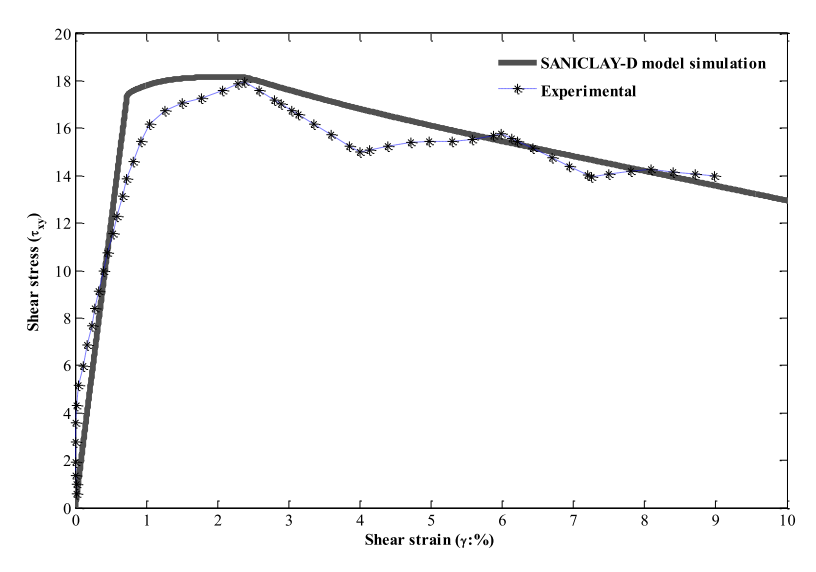


Fig. 8. Verification of SANICLAY-D model simulation and experimental stress-strain curves for the DSS test. (Data from Lefebvre and Pfendler 1996.)

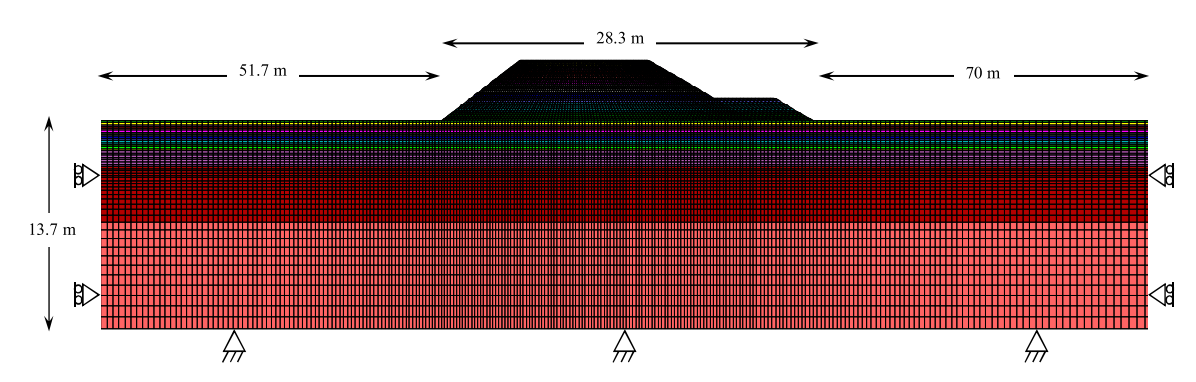


Fig. 9. Finite-difference mesh and boundary conditions of the simulated Test Embankment A.

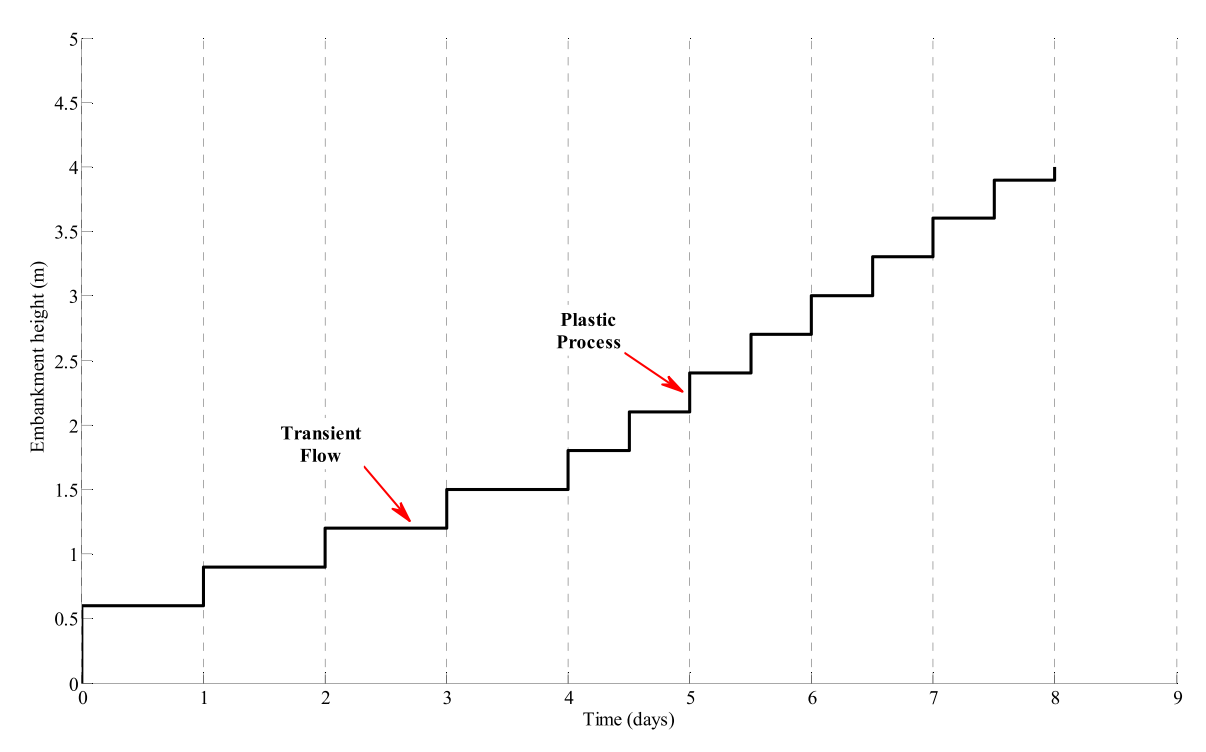


Fig. 10. Construction sequence of Test Embankment A.

constitutive models accompanied with field observations, as presented in Fig. 11.

The predictions of the three models for vertical displacements at both locations are reasonable up to an embankment height of 2.4 m. Until this height of the embankment, the simulated behavior in all cases at the locations of R23 and R18 and the adjacent regions is probably elastic and the stress path in the soil elements in this region is inside the YS. However, in none of the cases is the acceleration of the displacements at an embankment height of 2.7 m correctly simulated. This is due to the lack of capability of these models to simulate plastic deformation from the early stages of loading. This deficiency can be remedied by employing the concept of bounding surface, as previous studies Zdravković et al. (2002) were successful in predicting the prefailure deformation using different bounding surface constitutive models.

Fig. 12 shows the comparison between the SANICLAY-D estimation and the field measurement for vertical displacement at settlement gauges of R23, R18, R13, R8, and R3 along the ground surface beyond the toe of the embankment. The locations of the aforementioned gauges are illustrated in Fig. 6. As can be seen, the predictions up to an embankment height of 2.7 m are satisfactory, but beyond that height, by construction of the rest of the embankment fill, the difference between the field data and the numerical predictions increases.

The SANICLAY-D model predicts the height of failure as 3.9 m, which is exactly the same as in field observations, although there are some differences between the numerical simulation and field measurements of displacements. However, the SANICLAY model predicts a failure height of 3.7 m, which is lower than field observations.

Fig. 13 shows the simulated horizontal displacements at the toe of embankment and the field measurements at the R6 and R9

Table 2. Nonassociated Mohr-Coulomb model parameters

$\gamma (kN/m^3)$	$E (kN/m^2)$	v	φ (°)	ψ (°)
19	10,000	0.3	44	22

gauges. This figure shows that the horizontal displacement prediction of the SANICLAY-D model is in good agreement with field measurements. However, the simulated displacement is slightly larger than the field data. This difference might be related to the 3D shape of the slip surface, although the numerical simulation is a 2D plane strain.

For all cases, the S_u profiles were assumed to be a triaxial compression (TC) profile in Fig. 5 (continuous line) and the K_0 and OCR profiles were fine-tuned to achieve such a profile for S_u . The K_0 and OCR profiles for the two anisotropic soil models are as shown in Fig. 14. The subsequent S_u calculated using the anisotropic models is almost equal. The required K_0 and OCR profiles for the MCC model to obtain the same value for S_u as anisotropic models are shown in Fig. 15. As can be seen, owing to the anisotropy, there is a considerable discrepancy between the K_0 and OCR profiles in the MCC model and the anisotropic models.

The analysis using the MCC model was conducted up to an embankment height of 6.0 m; nevertheless, no failure was observed and considerable incremental shear strain did not appear. However, according to the vectors of incremental displacement at this stage, the failure was near. After a height of 6.0 m, no further construction of the lifts was possible because of the limitation imposed by the embankment shape after this height. Back analysis shows that, in order to predict the actual failure height of 3.9 m, the TC profile for the MCC model should be close to the DSS profile obtained by the anisotropic models.

One can clearly conclude that the anisotropy has a crucial role in the failure height of the embankment, based on the closest TC profile.

Failure Surface

Fig. 16 shows the vectors of incremental displacements and illustrates the mechanism and the mass of failure for each case. The failure surface for each case was estimated from the contours of shear strain increment and velocity vectors (Fig. 16). As can be seen in Fig. 17, the failure surface predicted by the

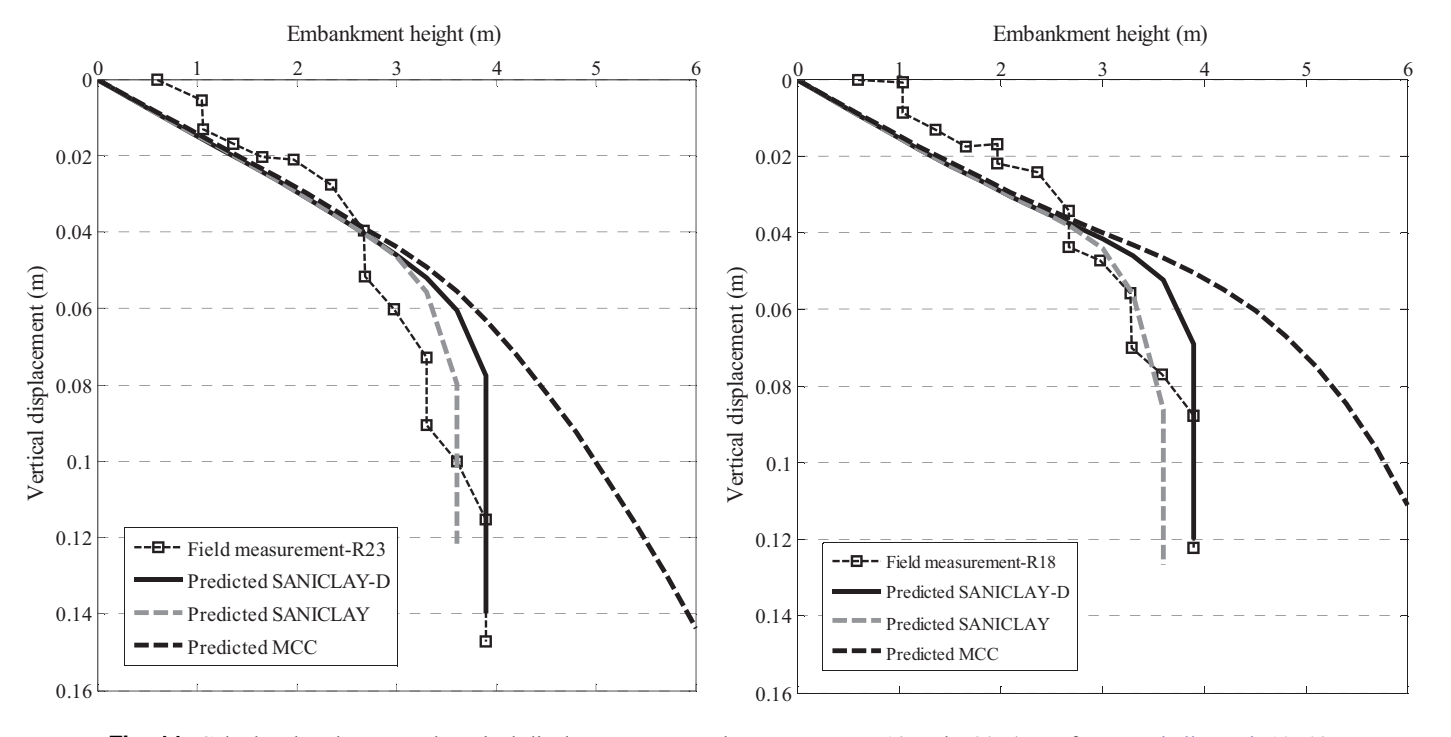


Fig. 11. Calculated and measured vertical displacements at settlement gauges R18 and R23. (Data from Rochelle et al. 1974.)

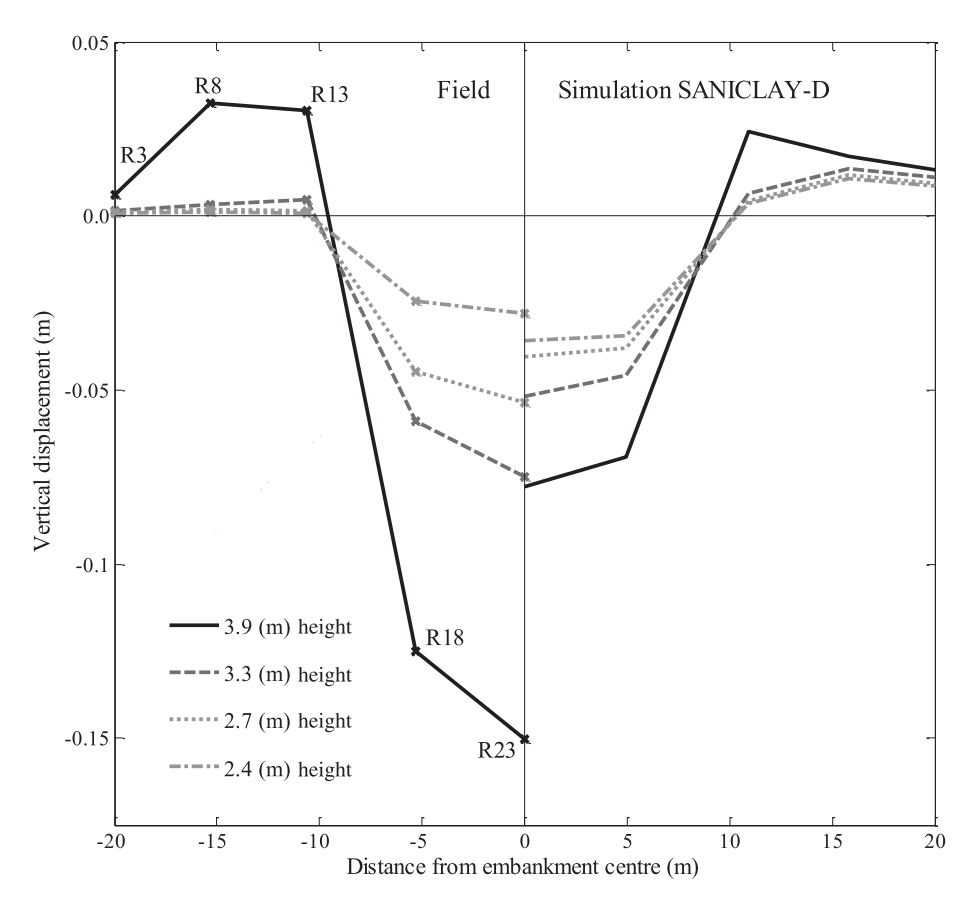


Fig. 12. Measured and simulated vertical displacements at different height of Test Embankment A. (Data from Rochelle et al. 1974.)

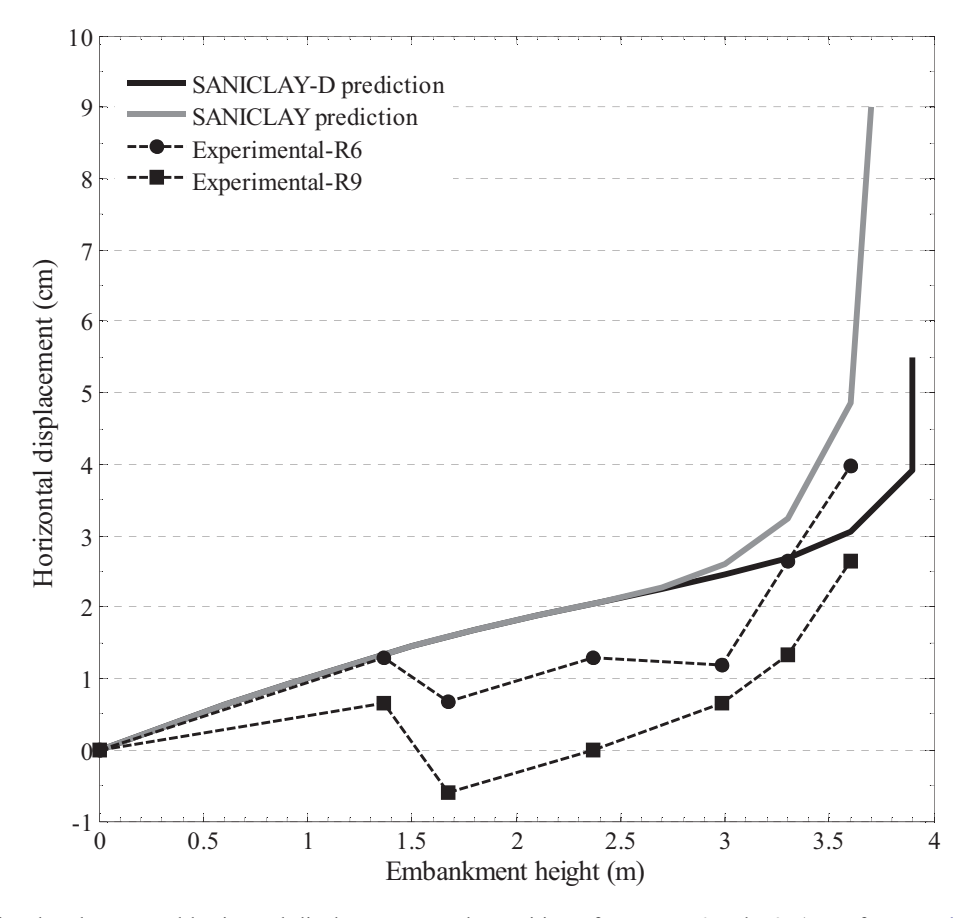


Fig. 13. Calculated and measured horizontal displacements at the position of gauges R6 and R9. (Data from Rochelle et al. 1974.)

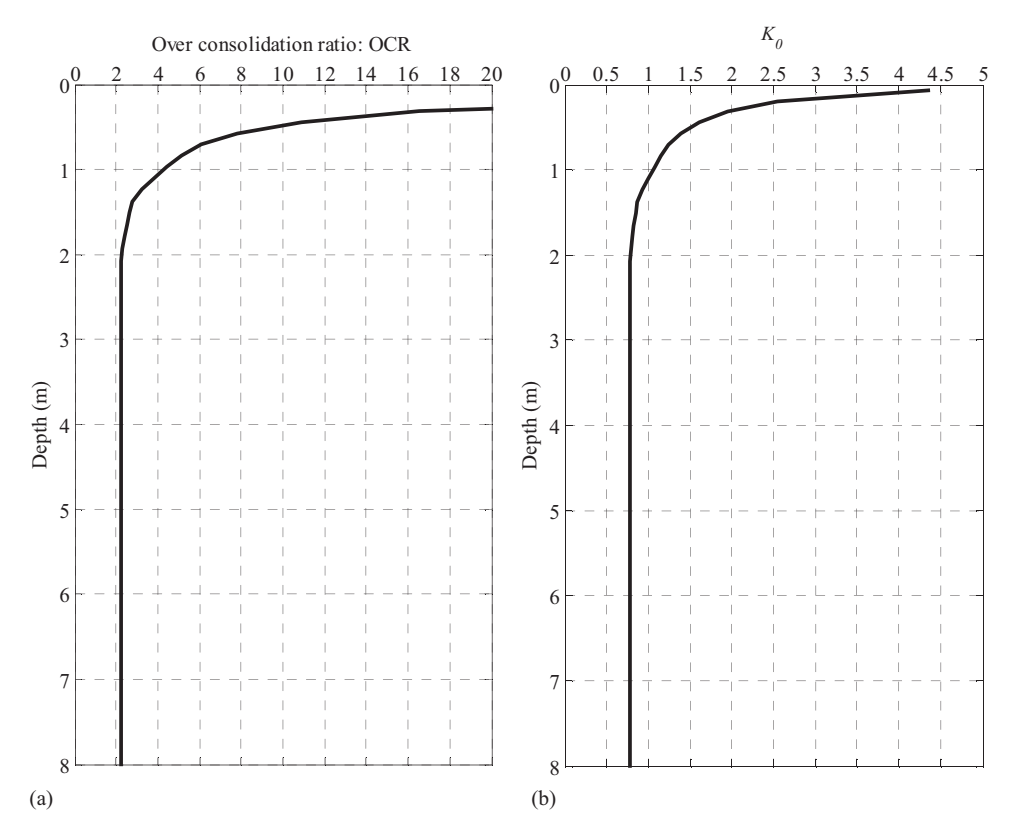


Fig. 14. (a) OCR profile; and (b) K_0 profile of the Saint-Alban clay deposits used in numerical simulation with the SANICLAY-D and SANICLAY models.

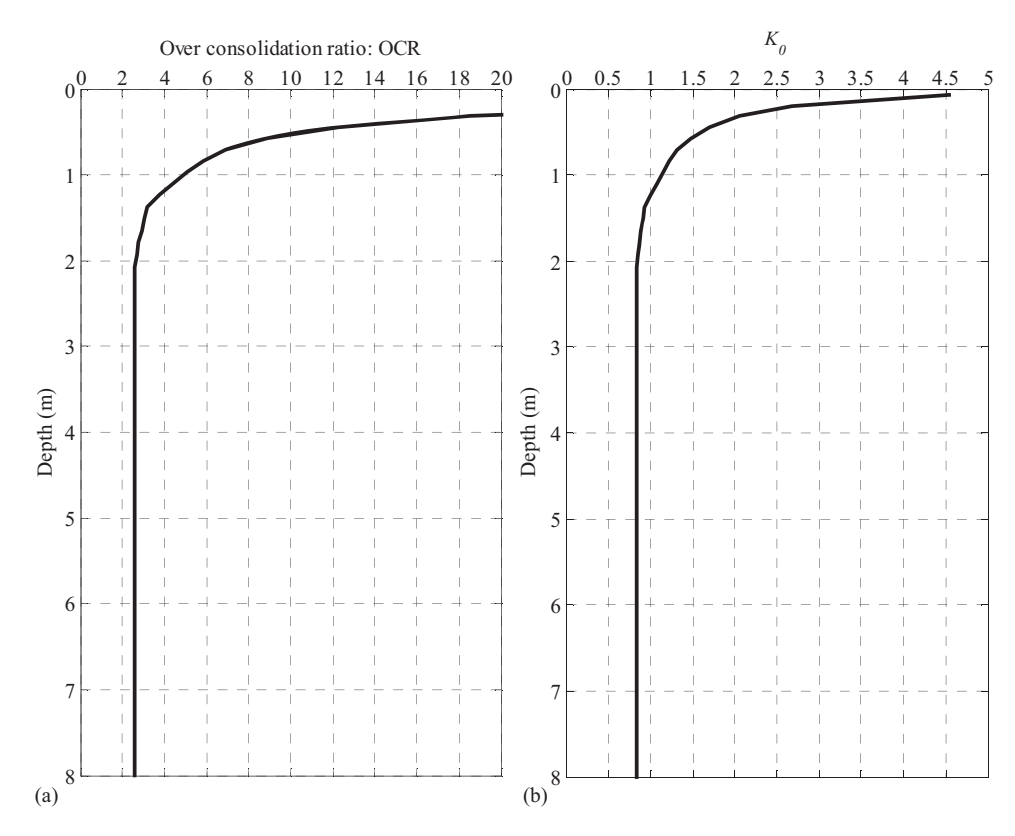


Fig. 15. (a) OCR profile; and (b) K_0 profile of the Saint-Alban clay deposits used in numerical simulation with the MCC model.

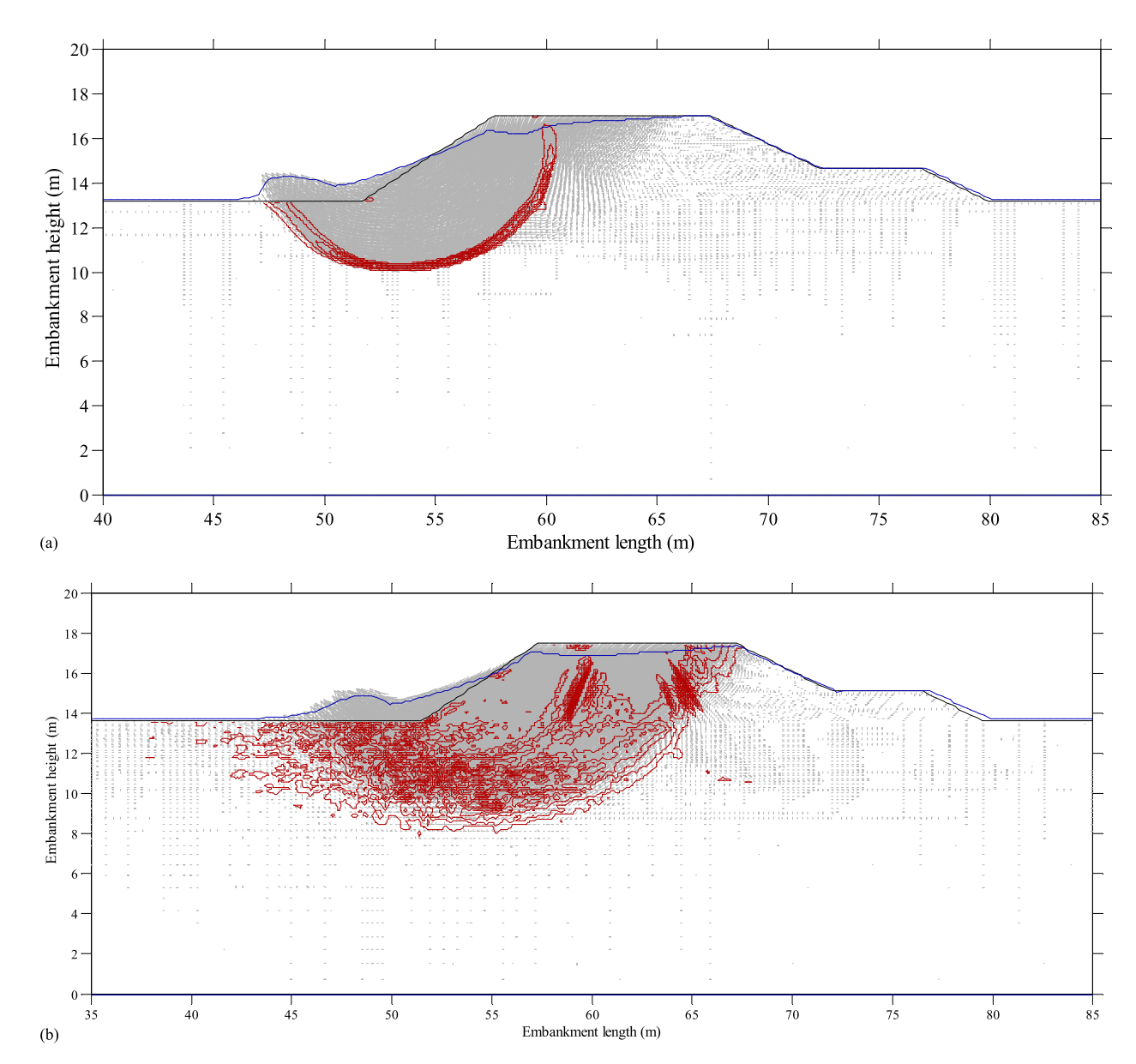


Fig. 16. Shear strain increment and incremental displacement vectors at failure using (a) SANICLAY-D; and (b) SANICLAY models.

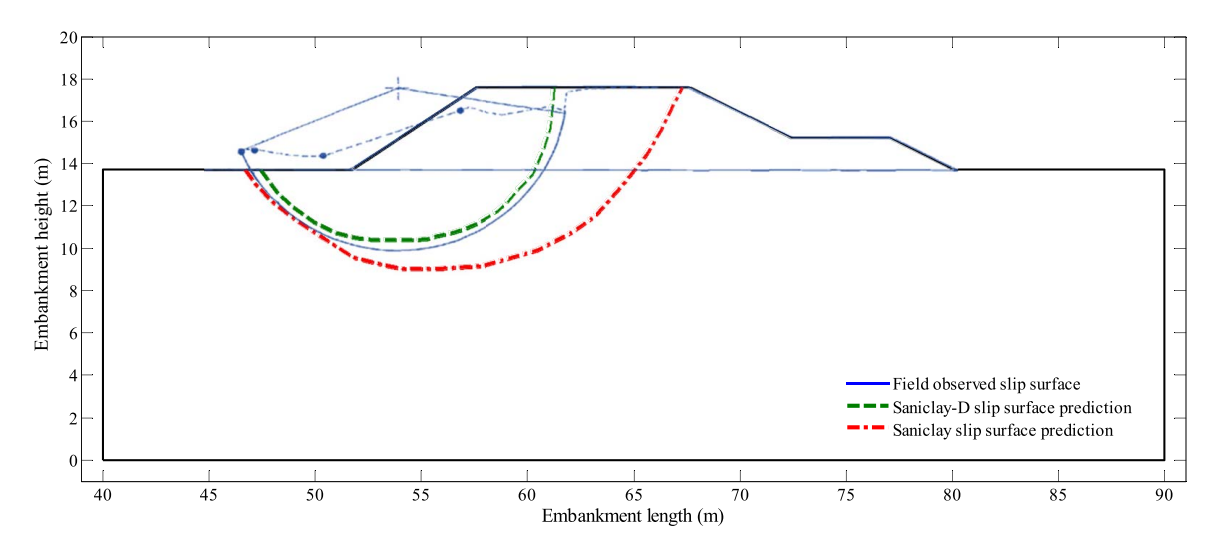


Fig. 17. Compression of slip surface prediction of SANICLAY-D and SANICLAY models with observed slip surface in the field. (Data from Rochelle et al. 1974.)

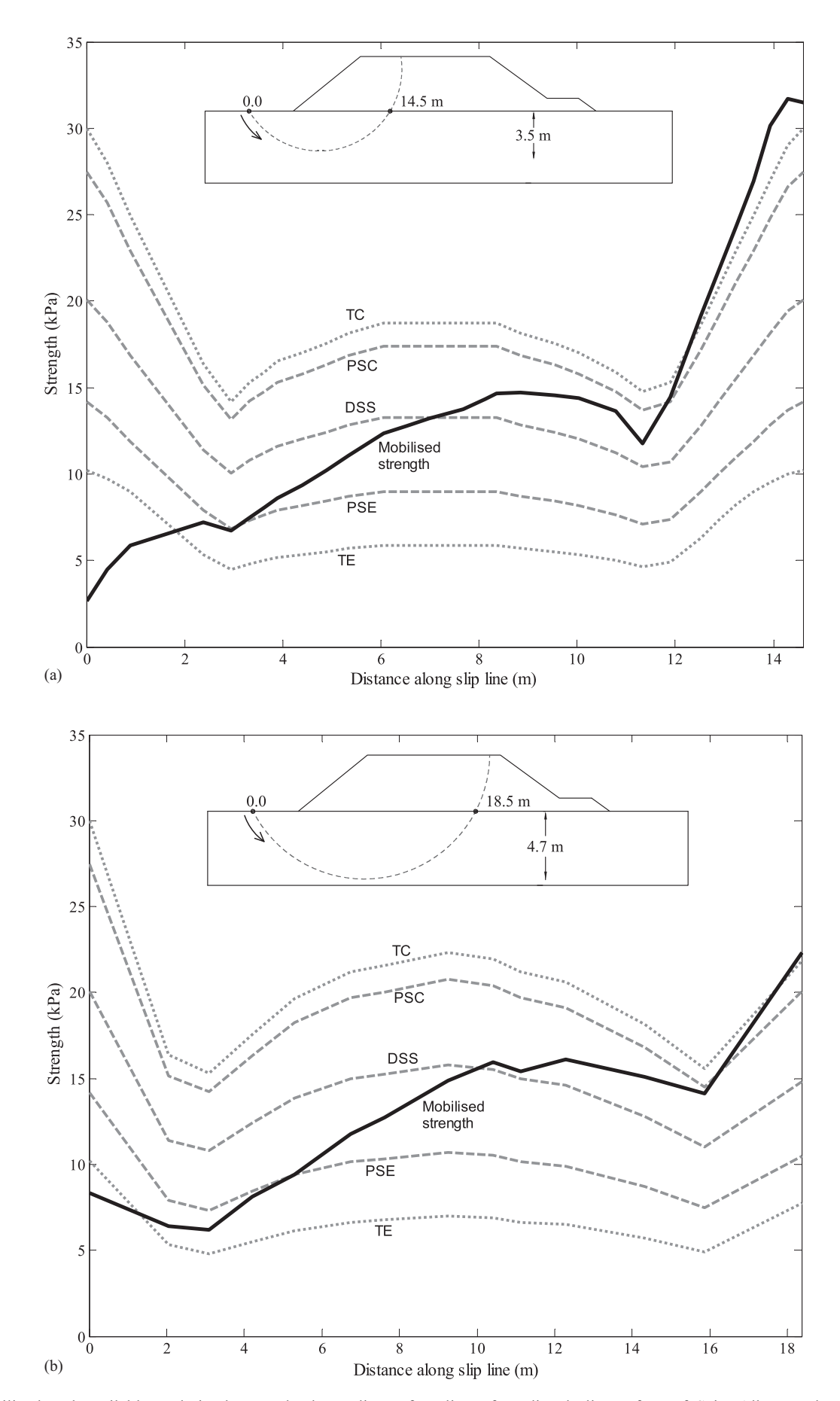


Fig. 18. Mobilized and available undrained strength along slip surface line of predicted slip surface of Saint-Alban Embankment A using (a) SANICLAY-D; and (b) SANICLAY model (anisotropic analysis).

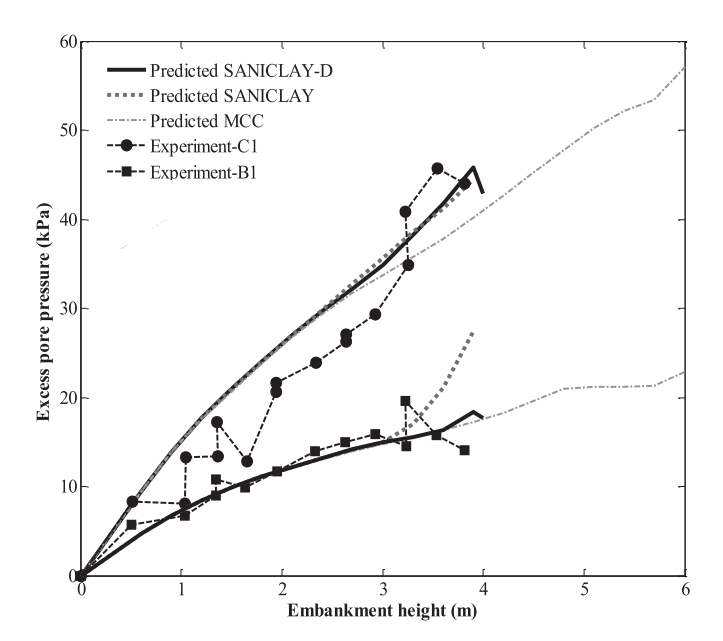


Fig. 19. Calculated excess pore water pressure against field measured values. (Data from Rochelle et al. 1974.)

SANICLAY-D model extends to a depth of 3.5 m from the ground surface and is remarkably consistent with the failure surface observed in the field by Rochelle et al. (1974), with a failure depth of 3.8 m. Conversely, the predicted failure surface, in the case that the decay of the soil structure is not accounted for, is considerably different from the actual failure surface. The depth of failure with the SANICLAY model was found to be 4.7 m. It is interesting to note that, despite the good performance of the SANICLAY model in predicting the failure height of the embankment, the estimated slip surface has a larger deviation from the field observation.

Fig. 18 shows the mobilized S_u along the slip surface calculated by the SANICLAY and SANICLAY-D models. As can be seen, the strength anisotropy is fully at work and the value of S_u changes with respect to the direction of loading. In this case, the value of S_u decreases from TC and plane stress compression (PSC) underneath the embankment to plane stress extension (PSE), beneath the toe. As shown in Fig. 18, the value of S_u beneath the toe calculated by the SANICLAY-D model is less than the triaxial extension (TE) strength. This is because, before the complete development of the slip surface, most of the soil structure in this area decays, as the stress path reaches the YS much earlier than the other areas along the slip surface. This may cause the deformations to localize in this region first and then spread to the embankment and the ground underneath it.

Based on the aforementioned results, it can be found that incorporation of the soil structure makes the slip surface narrower and shallower; the same conclusion made by Grammatikopoulou et al. (2007, 2008) and Panayides et al. (2012). In summary, the destructuration has a drastic effect on the depth and shape of the failure zone and should be taken into account in the soil constitutive model.

Excess Pore Water Pressure

Excess pore water pressure was monitored at two locations, namely C1 and B1, underneath the toe (Fig. 6), with pneumatic and electric vibrating wire piezometers, respectively. The computed excess pore water pressure with the three soil models for these locations

is presented in Fig. 19. The excess pore water pressures in all cases are the same up to an embankment height of 2.4 m. Beyond this height, the pore water pressure response in each case begins to diverge. It can be seen that the response in terms of excess pore water pressure is ascending up to failure. Fig. 19 also depicts a better functionality for the SANICLAY-D model beyond an embankment height of 2.4 m until failure.

Conclusions

Numerical analyses were performed for Test Embankment A, constructed on the soft Champlain clay in eastern Canada. To study the effect of the decay of the soil structure and the incorporation of the anisotropic strength on the behavior of the embankment, the soft foundation soil was modeled using three soil models: the SANICLAY-D model, which accounts for both features; the SANICLAY model, which only includes strength anisotropy; and the MCC model, with neither of the two features. By properly setting some state and material parameters of the SANICLAY-D model, the other two soil models could be activated. The constitutive models were implemented in FLAC code with a very simple integration scheme, called the *semiexplicit single-step plastic correction method*, which requires a small size for the time step in explicit calculations.

The results of numerical modeling, including vertical and horizontal displacements, slip surface shape, and excess pore water pressure, were compared with the field monitoring data. Overall, the predictions of the simple anisotropic constitutive models (the SANICLAY-D and SANICLAY models) agree reasonably well with the field measurements. It is demonstrated that in order to correctly predict the failure height of the embankment based on the undrained shear strength and initial conditions of the soil profile, which have been obtained through field and laboratory experiments, an anisotropic constitutive model should be adopted. In this regard, the SANICLAY-D and SANICLAY models were shown to be successful; the SANICLAY-D model prediction of the failure height of the embankment is about 3.9 m, which is perfectly consistent with the observed failure on the field. The SANICLAY model prediction is about 3.7 m, which is acceptable, whereas the classical MCC model gave the failure height as higher than 6 m.

It is also shown that ignoring the soil structure and the destructuration alters the shape of the modeled failure surface. The failure surface predicted by the SANICLAY model is longer and deeper than the one calculated via the SANICLAY-D model, which was remarkably close to the slip surface recorded in the field. Zdravković et al. (2002) and Panayides et al. (2012) analyzed the same boundary value problem as in this study with advanced and complex bounding surface models, namely the MIT-E3 and KHCM models, respectively, and estimated a failure surface with a shape notably different from the one observed on the site. They attributed this discrepancy to the 3D behavior of the actual embankment. Therefore, it would be interesting to examine the performance of the SANICLAY-D model in a 3D numerical analysis of the embankment.

It was also found that the only shortcoming of the simple anisotropic models was their weakness in accurately reproducing the field deformation. This deficiency may be remedied by employing, for instance, the concept of a bounding surface (Dafalias 1986b) for the extension of the simple models. This extension should be made in such a way that the deformation prediction of the models is improved, while the simplicity of their implementation in the numerical code is also maintained.

Appendix. Destructuration Hardening Rules of SANICLAY-D

For the sake of completeness of presentation, some of the key components of the SANICLAY-D model that are not presented in the main body of this paper are summarized here. The SANICLAY-D model comprises four hardening rules, namely two destructuration rules, and one isotropic hardening rule, which are described next, as well as one rotational hardening rule, presented in Eq. (5). The evolution rule for S_i and S_f describes, respectively, the isotropic and frictional destructuration. Both of the destructuration rules are decreasing functions of plastic strain and are expressed as follows (Taiebat et al. 2010):

$$\dot{S}_i = -k_i \left[\frac{(S_i - 1)\dot{\varepsilon}_d}{(\lambda^* - \kappa^*)} \right] \tag{10}$$

$$\dot{S}_f = -k_f \left[\frac{(S_f - 1)\dot{\varepsilon}_d}{(\lambda^* - \kappa^*)} \right] \tag{11}$$

where λ^* and κ^* = slopes of the compression and the swelling lines in a volumetric strain–logarithmic mean stress compression plane, respectively; and k_i and k_f = model parameters that control the rate of isotropic and frictional destructuration, respectively. The variable $\dot{\varepsilon}_d$ i= rate of damage strain and is defined as a function of plastic volumetric and plastic shear strains (Taiebat et al. 2010):

$$\dot{\varepsilon}_d = \left[(1 - A)(\dot{\varepsilon}_v^p)^2 + A \left(\frac{2}{3} \dot{\varepsilon}_s^p : \dot{\varepsilon}_s^p \right) \right]^{1/2} \tag{12}$$

where A = nondimensional material parameter and controls the relative effectiveness of the plastic volumetric (\dot{e}^p_v) and deviatoric plastic strains (\dot{e}^p_s) . Also, the plastic volumetric and plastic shear strains can be calculated as

$$\dot{\varepsilon}_{v}^{p} = tr[\dot{\varepsilon}^{p}], \qquad \dot{\varepsilon}_{s}^{p} = \dot{\varepsilon}^{p} - \frac{1}{3}\dot{\varepsilon}_{v}^{p}I \tag{13}$$

where $\dot{\boldsymbol{\varepsilon}}^p$ = plastic strain tensor.

The last hardening rule corresponds to the variation in the size of the intrinsic YS (p_0) with plastic volumetric strain rate and is given by (as in the MCC model)

$$\dot{p}_0 = \frac{p_0}{\left(\lambda^* - \kappa^*\right)} \dot{\varepsilon}_{\nu}^p \tag{14}$$

The elastic response is assumed to be isotropic and is divided into volumetric and deviatoric parts:

$$\dot{p} = K\dot{\varepsilon}_{\nu}^{e}, \qquad \dot{s} = 2G \left[\dot{\varepsilon}^{e} - \frac{1}{3} tr[\dot{\varepsilon}^{e}] I \right]$$
 (15)

where K and G = bulk and shear moduli, respectively, and are given by

$$K = \frac{p}{\kappa^*}, \qquad G = \frac{3K(1 - 2\nu)}{2(1 + \nu)}$$
 (16)

where v = Poisson's ratio.

Data Availability Statement

All data, models, and code generated or used during the study appear in the published article.

References

- Al-Tabbaa, A., and D. M. Wood. 1989. "An experimentally based bubble model for clay." In *Proc., 3rd Int. Symp. on Numerical Models in Geomechanics*, 91–99. Amsterdam, Netherlands: Elsevier.
- Andresen, L., G. Saygili, and G. Grimstad. 2011. "Finite element analysis of the Saint-Alban embankment failure with an anisotropic undrained strength model." In *Proc., 15th European Conf. of Soil Mechanics and Geotechnical Engineering*, 1111–1118. https://doi.org/10.3233/978-1-60750-801-4-1111.
- Baudet, B., and S. Stallebrass. 2004. "A constitutive model for structured clays." *Géotechnique* 54 (4): 269–278. https://doi.org/10.1680/geot .2004.54.4.269.
- Cotecchia, F., and R. J. Chandler. 2000. "A general framework for the mechanical behaviour of clays." *Géotechnique* 50 (4): 431–447. https://doi.org/10.1680/geot.2000.50.4.431.
- Dafalias, Y. F. 1986a. "An anisotropic critical state soil plasticity model." Mech. Res. Commun. 13 (6): 341–347. https://doi.org/10.1016/0093 -6413(86)90047-9.
- Dafalias, Y. F. 1986b. "Bounding surface plasticity. I: Mathematical foundation and hypoplasticity." *J. Eng. Mech.* 112 (9): 966–987. https://doi.org/10.1061/(ASCE)0733-9399(1986)112:9(966).
- Dafalias, Y. F., M. T. Manzari, and A. G. Papadimitriou. 2006. "SANICLAY: Simple anisotropic clay plasticity model." *Int. J. Numer. Anal. Methods Geomech.* 30 (12): 1231–1257. https://doi.org/10.1002/nag.524.
- Dafalias, Y. F., and M. Taiebat. 2013. "Anatomy of rotational hardening in clay plasticity." *Géotechnique* 63 (16): 1406–1418. https://doi.org/10.1680/geot.12.P.197.
- Dafalias, Y. F., M. Taiebat, F. Rollo, and A. Amorosi. 2020. "Convergence of rotational hardening with bounds in clay plasticity." *Géotech. Lett.* 10 (1): 16–19. https://doi.org/10.1680/jgele.19.00012.
- Gens, A., and R. Nova. 1993. "Conceptual bases for a constitutive model for bonded soils and weak rocks." In *Int. Conf. on Hard Soils—Soft Rocks*, 485–494. Rotterdam, The Netherlands: A A Balkema.
- Grammatikopoulou, A., L. Zdravkovic, and D. M. Potts. 2007. "The effect of the yield and plastic potential deviatoric surfaces on the failure height of an embankment." *Géotechnique* 57 (10): 795–806. https://doi.org/10.1680/geot.2007.57.10.795.
- Grammatikopoulou, A., L. Zdravkovic, and D. M. Potts. 2008. "Numerical analysis of an embankment founded on structured clay." In *Proc., 12th Int. Conf. on Computer Methods and Advances in Geomechanics 2008*, 4041–4048. Red Hook, NY: Curran.
- Hight, D. W. 1998. Anisotropy in soils: Its measurement and practical implications. Singapore: Nanyang Technological Univ., NTU-PWD Geotechnical Research Centre.
- Karstunen, M., H. Krenn, S. J. Wheeler, M. Koskinen, and R. Zentar. 2005. "Effect of anisotropy and destructuration on the behavior of murro test embankment." *Int. J. Geomech.* 5 (2): 87–97. https://doi.org/10.1061 //(ASCE)1532-3641(2005)5:2(87).
- Korhonen, K. H., and M. Lojander. 1987. "Yielding of Perno clay." In Proc., 2nd Int. Conf. on Constitutive Laws for Engineering Materials, 1249–1255. Amsterdam, Netherlands: Elsevier.
- Lambe, T. W., and R. V. Whitman. 1991. Soil mechanics. Hoboken, NJ: John Wiley & Sons.
- Lefebvre, G., and P. Pfendler. 1996. "Strain rate and preshear effects in cyclic resistance of soft clay." *J. Geotech. Eng.* 122 (1): 21–26. https://doi.org/10.1061/(ASCE)0733-9410(1996)122:1(21).
- Leroueil, S., D. Demers, and F. Saihi. 2001. "Considerations on stability of embankments on clay." *Soils Found.* 41 (5): 117–127. https://doi.org/10.3208/sandf.41.5 117.
- Mitschell, K. J., and K. Soga. 2005. Fundamentals of soil behaviour. Hoboken, NJ: John Wiley & Sons.
- Morti, J., and P. A. Cundall. 1982. "Mixed discretization procedure for accurate solution of plasticity problem." Int. J. Num. Method Eng. 6: 129–139.
- Newson, T. A., and M. C. R. Davies. 1996. "A rotational hardening constitutive model for anisotropically consolidated clay." *Soils Found*. 36 (3): 13–20. https://doi.org/10.3208/sandf.36.3_13.
- Panayides, S., M. Rouainia, and D. Muir Wood. 2012. "Influence of degradation of structure on the behaviour of a full-scale embankment." Can. Geotech. J. 49 (3): 344–356. https://doi.org/10.1139/t11-104.

- Potts, D. M., and A. Gens. 1984. "The effect of the plastic potential in boundary value problems involving plane strain deformation." *Int. J. Numer. Anal. Methods Geomech.* 8 (3): 259–286. https://doi.org/10.1002/nag.1610080305.
- Quigley, R. M. 1980. "Geology, mineralogy, and geochemistry of Canadian soft soils: A geotechnical perspective." Can. Geotech. J. 17 (2): 261–285. https://doi.org/10.1139/t80-026.
- Razavi, S. K., M. Hajialilue Bonab, and A. Dabaghian. 2020. "Investigation into the internal erosion and local settlement of Esfarayen earth-fill dam." *J. Geotech. Geoenviron. Eng.* 146 (4): 04020006. https://doi.org/10.1061/(ASCE)GT.1943-5606.0002216.
- Rochelle, P. L., B. Trak, F. Tavenas, and M. Roy. 1974. "Failure of a test embankment on a sensitive Champlain clay deposit." *Can. Geotech. J.* 11 (1): 142–164. https://doi.org/10.1139/t74-009.
- Rotisciani, G. M., and S. Miliziano. 2014. "Guidelines for calibration and use of the Severn-Trent sand model in modeling cantilevered wall-supported excavations." *Int. J. Geomech.* 14 (6): 04014029. https://doi.org/10.1061/(ASCE)GM.1943-5622.0000373.
- Rouainia, M., and D. Muir Wood. 2000. "A kinematic hardening constitutive model for natural clays with loss of structure." *Géotechnique* 50 (2): 153–164. https://doi.org/10.1680/geot.2000.50.2.153.
- Rousé, P. C., D. A. Shuttle, and R. J. Fannin. 2006. "Implementation of critical state models within FLAC." In *Proc.*, 4th Int. FLAC Symp. on Numerical Modelling in Geomechanics-2006, 29–31. Minneapolis, MN: Itasca Consulting Group.
- Sheng, D., S. W. Sloan, and H. S. Yu. 1999. "Practical implementation of critical state models in FEM." In Proc., 8th Australia New Zealand Conf. on Geomechanics: Consolidating Knowledge. Sydney, NSW: Australian Geomechanics Society.
- Shirmohammadi, A., M. H. Bonab, and S. S. Shishvan. 2016. "Modified explicit scheme of return mapping integration algorithm on rotational hardening constitutive model for clay." Asian J. Civ. Eng. 17 (1): 43–57.

- Smith, P. R., R. J. Jardine, and D. W. Hight. 1992. "The yielding of Bothkennar clay." *Géotechnique* 42 (2): 257–274. https://doi.org/10 .1680/geot.1992.42.2.257.
- Taiebat, M., Y. F. Dafalias, and R. Peek. 2010. "A destructuration theory and its application to SANICLAY model." Int. J. Numer. Anal. Methods Geomech. 34 (10): 1009–1040. https://doi.org/10.1002/nag.841.
- Tavenas, F. A., C. Chapeau, P. L. Rochelle, and M. Roy. 1974. "Immediate settlements of three test embankments on Champlain clay." Can. Geotech. J. 11 (1): 109–141. https://doi.org/10.1139/t74-008.
- Tavenas, F. A., P. Jean, P. Leblond, and S. Leroueil. 1983. "The permeability of natural soft clays. Part II: Permeability characteristics." Can. Geotech. J. 20 (4): 645–660. https://doi.org/10.1139/t83-073.
- Tavenas, F. A., and S. Leroueil. 1977. "Effect of stresses and time on yielding of clays." In *Proc.*, 9th Int. Conf. on Soil Mechanics and Foundation Engineering, 319–326. Berlin, Germany: Springer.
- Thevanayagam, S., and J.-L. Chameau. 1992. "Modeling anisotropy of clays at critical state." *J. Eng. Mech.* 118 (4): 786–806. https://doi.org/10.1061/(ASCE)0733-9399(1992)118:4(786).
- Trak, B., P. L. Rochelle, F. Tavenas, S. Leroueil, and M. Roy. 1980. "A new approach to the stability analysis of embankments on sensitive clays." *Can. Geotech. J.* 17 (4): 526–544. https://doi.org/10.1139/t80-061.
- Wheeler, S. J., A. Näätänen, M. Karstunen, and M. Lojander. 2003. "An anisotropic elastoplastic model for soft clays." *Can. Geotech. J.* 40 (2): 403–418. https://doi.org/10.1139/t02-119.
- Whittle, A. J., and M. J. Kavvadas. 1994. "Formulation of MIT-E3 constitutive model for overconsolidated clays." *J. Geotech. Eng.* 120 (1): 173–198. https://doi.org/10.1061/(ASCE)0733-9410(1994) 120:1(173).
- Zdravković, L., D. M. Potts, and D. W. Hight. 2002. "The effect of strength anisotropy on the behaviour of embankments on soft ground." *Géotechnique* 52 (6): 447–457. https://doi.org/10.1680/geot.2002.52.6.447.